ISSN 1330-3651 (Print), ISSN 1848-6339 (Online) https://doi.org/10.17559/TV-20200926203404
Original scientific paper

Numerical and Experimental Study of Solar Dryer Equipped with PV/T

Mohamed FTERICH*, Houssam CHOUIKHI, Salmen GHORBEL, Hatem BENTAHER, Sadoth SANDOVAL-TORRES, Aref MAALEJ

Abstract: Drying of agricultural food products in a solar dryer equipped with a PV/T air collector is a frequent research topic. Consequently, an experimental and numerical study has been conducted on MSD to examine the distribution of the temperature and airflow. Moreover, COMSOL Multiphysics software is used to solve a 3D temporal non-isothermal flow for the system invented. Further, the improvement of the mass flow rate dropped approximately the average PV temperature experimentally from 60 °C to 43 °C and from 63 °C to 47 °C numerically. Furthermore, the average outlet temperature of the PV/T reaches 60,5 °C in the experience and 62 °C in the simulation in the case where the mass flow rate is 0,012 kg/s, but it is dropped to 44 °C in the experience and 45 °C in the simulation for the highest mass flow rate of 0,0235 kg/s. Hence, the best recorded average thermal efficiency of the PV/T was 53% for the maximum mass flow rate (0,025 kg/s), while the average thermal efficiency of the PV/T was 29% when the mass flow rate decreased to 0,012 kg/s. Consequently, the recorded temperature in the drying chamber reaches 55 °C in the experimental data and in the simulation.

Keywords: experimental; forced convection; PV/T air collector; simulation and COMSOL Multiphysics; solar dryer; solar energy

1 INTRODUCTION

The research on dryers has a long tradition; it is the best major technology of food conservation; however, it consumes around 10% to 15% of the industry's total energy [1]. Moreover, the scarcity of energy in the world, on one hand, and the increase of the fossil energy cost on the other hand, caused the researchers to look for alternatives to fossil energy. The use of renewable energy in drying has become a necessary alternative [2]. Consequently, this technology takes up appreciable dominance and requires enhancement and development to the highest possible extent [3]. Improving the performance of solar dryers could provide the required energy for drying food products [4]. Hence, the drying efficiency has been enhanced by using the solar collector integrated with the drying room as the photovoltaic hybrid solar collector (PV/T), [5].

Solar drying with forced convection is one of the best applications of PV/T due to the need of high temperature and electrical energy to generate the fans rotation. Hence, drying food products in a solar dryer equipped with a PV/T air collector is a topic of frequent research [6]. Consequently, in the past several decades, several types and designs of solar dryers have been studied. In this paper, the analysis of previous studies concentrated on solar dryers equipped with solar collectors is presented. The mixed solar dryer (MSD) consists in drying the product simultaneously by direct radiation through the transparent walls and by the convection of heat from the solar collector [7]. César et al. [8] reported a global performance of their MSD of 10,66% [8]. Elkhadraoui et al. [9] built and tested a MSD for drying red pepper and sultana grape. The moisture content of the red pepper was reduced to 16% WB (wet basis) in 24 hours for open drying, while the combination dryer only took 17 hours. Sreekumar et al. [10] realized a solar dryer to dry the bitter gourd having an initial moisture content of 95%. The moisture content was reduced to 5% WB in 11 hours for OSD, while the invented dryer only took 6 hours. Kam et al. [11] studied a solar dryer with natural convection. They have concluded that the temperatures tolerated for drying fruits and vegetables are between 30 °C and 80 °C. Consequently, the temperature obtained inside the studied dryer was 60 °C. Kuan et al. [12] reported that the drying rate was enhanced by more than 30% in the dryer equipped with solar collectors compared to the open solar one. Daghigh et al. [13] concluded that the average efficiency of the dryer with PV/T was 13,7% and the drying time was 11 hours with a temperature of 45 °C, but it dropped to 8,5 hours with 55 °C. Lakshmi et al [14] evaluated a MSD. The results reveal that the desired moisture content (5,3% DB) was reached within 330 minutes in the MSD, while the OSD took 870 minutes. Moreover, the MSD reduces the drying time by 62% and improves the quality of the dried product.

The drying kinetics are faster using a solar dryer with solar collectors [15]. The drying process is in direct relation with both working parameters of the dryer (temperature, air speed and humidity) and geometrical characteristics of the product which are both used to calculate convection coefficient. Other scientific studies showed that the drying of the product when the drying temperature and the air speed increased is faster but not instantaneous and that a response time is recorded. Moreover, the drying temperature is an influential external parameter which is not the case of air velocity and humidity [16]. Dhalsamant et al. [17] have observed that the coefficient of convection was largely affected by shrinkage parameter followed by sample diameter. Also, they concluded that taking into account the shrinkage of the sample led to an overestimation of the coefficient of convection values in the range of 55,72% - 61,86%. Comparing our results with other scientific research shows that there is an improvement in the thermal efficiency of the PV/T and the drying temperature due to the heat absorbed from the PV panel. Consequently, the average thermal efficiency recorded is 53 % and drying temperature 55 °C. However, in recent times, many researchers experimentally and theoretically studied the performance of PVT air collectors. Their result showed that the thermal performance was 31 % in [18] but it reached 40 % [19] and it improved to 56 % in [20]. Further, drying temperature varied from 40 °C to 51 °C, [18-20].

This research constitutes a relatively new area in the technology of solar drying. In the present work, MSD was studied experimentally, and then related equations were numerically solved. The numerical simulations are

compared with experimental results and then used to investigate the temperature and air flow distribution inside the studied solar dryer. Numerical resolutions take into account the local metrological conditions of Sfax-Tunisia and the impact of the airflow speed on the efficiency of the MSD is studied. The major purpose of the present study is to evaluate the thermal performance of the MSD to dry the agro-food products. Moreover, the thermal efficiency of the solar collector, as well as the outlet temperature and drying temperature inside the MSD were studied.

2 SYSTEM DESCRIPTION

2.1 Experimental Framework

The studied solar dryer in this paper, shown in Fig. 1, consists of two parts: a drying chamber which contains the product spread on the trays and a PV/T air collector with a surface area of 1,4 m² presented in Fig. 2 which converts solar radiation into heat recovered by the air, when it circulates in the gap and the tubes under the action of a fan. The hot air rises by forced convection to the drying chamber, then it leaves the dryer to the outside. The drying time is very variable depending on climatic conditions. The chamber of our prototype is constructed by an Aluminium metal structure and multi-layer polycarbonate plates to allow the passage of solar radiation inside the chamber. The dimensions ($L \times W \times H$) of the structure are 1,81 × 0,81 × 0,75 m respectively. On the front side, there are two doors for loading and unloading the products to be dried. At the roof level, a fan (80 W, 12 V) is placed to ensure the evacuation of humid air and speed up the drying operation. The choice of the airflow direction, from bottom to top, aims to enhance the natural convection.

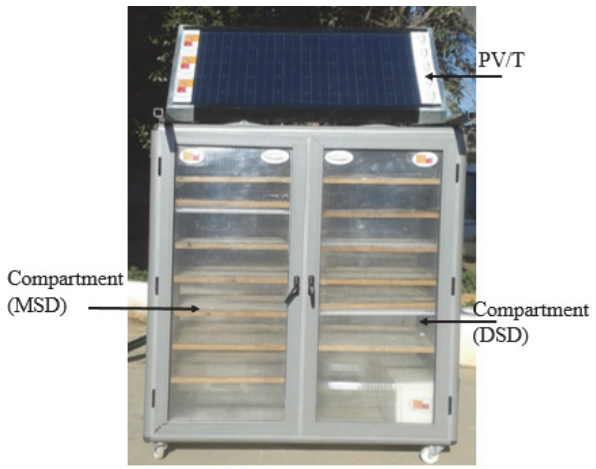

Figure 1 Solar dryer design

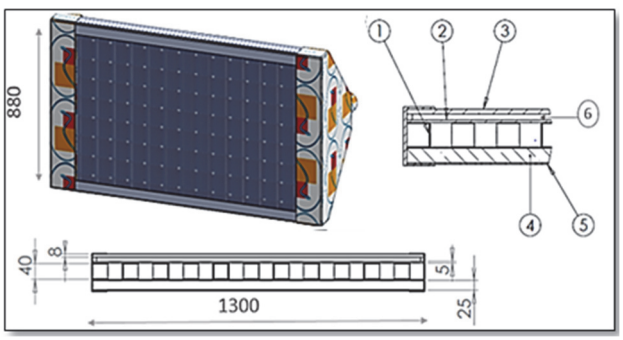

Figure 2 Solar collector (PV/T): (1) Aluminum tube, (2) PV panel, (3) Glass, (4) Insulator, (5) Aluminum sheet, and (6) Gap

The parameters controlled were saved: solar irradiation, ambient temperature, temperature of the PV panel, gap air temperature, glass temperature, outlet air temperature, and air velocity in the drying room. At the level of the solar PV/T air collector, many sensors of thermocouples type J were placed to evaluate the temperatures. The drying temperatures at the trays, the outlet temperature of the chamber was measured using DHT22.

Table 1 Equipment used in the experiment

Sensor/Type	Reference	Sensitivity	Accuracy
Pyranometer	CIMEL CE 1180	12,29 µV/Wm²	±1 W/m²
Thermocouple type J	N.I.S.T- ITS-90	10 µV/°C	±0,8%
Anemometer	KIMO TH 100-AOD	0,01 m/s	±1,8%
Data Logger	HP-Agilent 34970A	1 Vpp	0.004% basic DCV
DHT22	DHT22	0,1 °C and 0,1%	±0,6 °C, ±1,8%

The places of the measurements are shown in Fig. 3. In the horizontal plane of the panel, we fixed a pyranometer to measure the solar radiation. The air velocity is one of the principal factors which affect the solar drying process; however, an experimental study on the homogeneity of the air in the trays was carried using the anemometer.

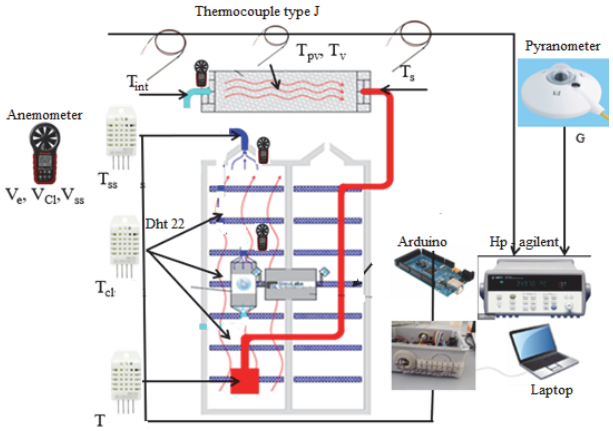

Figure 3 Schematic diagram showing temperature sensors position in the solar drying setup

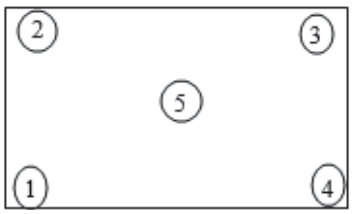

Figure 4 Velocity measurement points at the tray

The measurement points of the velocity with anemometer are shown in Fig. 4. The experimental results are saved using data logger Hp-Agilent and Arduino.

2.2 Numerical Solution

Fig. 5 shows the three-dimensional prototype of the solar dryer studied. This conception consists of two compartments, the PV/T and the drying room. However, Tab. 2 shows the properties of the materials used in the

simulation [21-23]. In addition, the parameters were applied in the simulation model shown in Tab. 3 and Tab. 4. Moreover, according to Tab. 5, the flow in the dryer is always laminar.

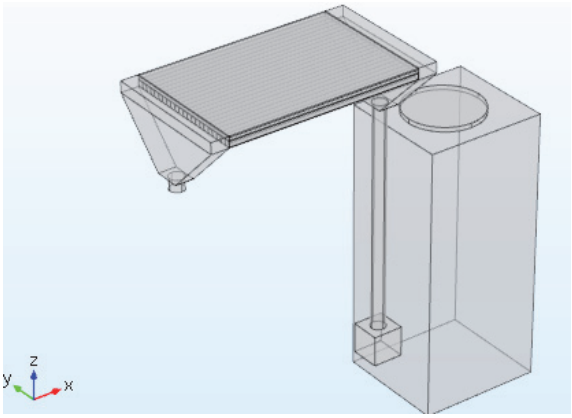

Figure 5 3D Geometry of solar dryer: (1) PV/T, (2) Drying chamber

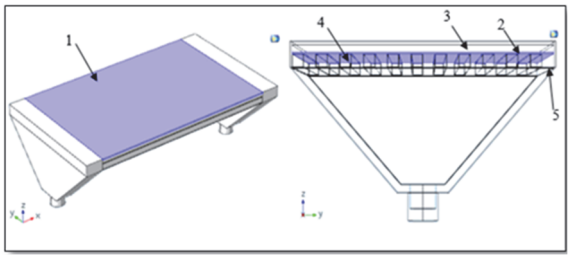

Figure 6 3D Geometry of PV/T air collector, (1) Glass cover, (2) PV panel, (3) Air gap, (4) Aluminum tube and (5) Aluminum sheet

Table 2 Dryer materials properties

Materials	ρ / kg/m^3	K / W/mK	C_p / J/kgK
Glass	2200	1,8	850
PV-Panel	2329	130	700
Aluminum	2700	160	900

Table 3 Parameters used in the model

Parameters	Value
ε_v	0,88
α_v	0,066
τ_v	0,95
ε_{pv}	0,95
α_{pv}	0,85
τ_{pv}	0,87
σ / W/m^{2}K^4	5,670373e^{-8}

Table 4 Non-dimensional numbers used in the model

Parameters	Expression
L_{eq} / m	$(4A_v)/P$
Re	$\rho \cdot u \cdot D_h / \mu$
Nu	$0,664\left(Re^{0,5}\right)\left(Pr^{1/3}\right)$
Pr	0,728

Table 5 Number of Reynolds in the tube of the PV/T

Air velocity / m/s	Flow rates / kg/s	Re
0,5	0,0009312	310
2	0,003724	1243

3 MODELLING OF SOLAR DRYER

The three-dimensional study is a little more complex but nevertheless emblematic. Mathematical expressions in 3D mode are written below. The resolution method is based on the following approaches and simplifications. A non-isothermal laminar flow physics was used in the model invented. The parameters used in the numerical model are shown in Tab. 3 and the non-dimensional numbers utilized in our model are introduced in Tab. 4. The following assumptions were used to simplify the simulation:

1. The phases are in thermodynamic equilibrium,
2. The temperature of two faces of the PV panel are in equilibrium,
3. There are no air leaks,
4. The fluid is incompressible,
5. The airflow is laminar,
6. The top surface of the glass is clean from the dust allowing absorption of more of the solar radiation,
7. The air circulates in the drying chamber in the vertical direction and its speed is uniform throughout the chamber,
8. The pressure inside the dryer is taken equal to atmospheric pressure,
9. The physical properties of the materials are considered constant,
10. The airflow speed is uniform in the tubes and the PV gap, its local state depends only on one side,
11. Air is an ideal gas,
12. The physical properties of the circulating air were independent of temperature and pressure, so the air can be considered an incompressible fluid.

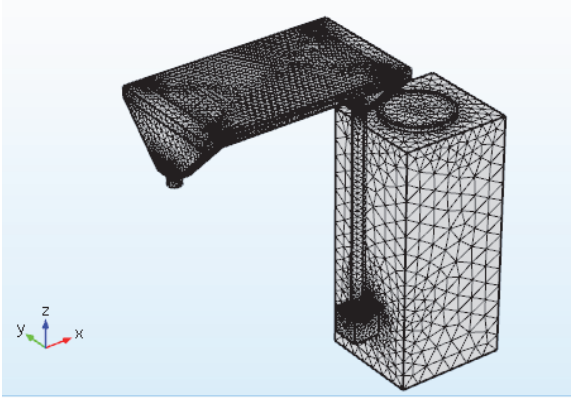

Figure 7 3D mesh sequence

The fluid flow and heat transfer characteristics in the solar dryer equipped with PV/T were studied by means of computational fluid dynamics (CFD) calculations using the COMSOL Multiphysics software. A simplified meshed model was created in COMSOL Multiphysics software for analysis. The governing equations, including the energy equation, radiation model, and k-ε model, were chosen to test the suitability and the applicability of the model on the dryer.

In order to reduce the computational cost, we decided to use RANS (Reynolds-Averaged Navier-Stokes) formulation of the Navier-Stokes's equations, which averages the velocity and pressure fields in time. These time-averaged equations were computed in a stationary way on a relatively coarse mesh, significantly reducing the computing power and time required for such simulations. System equations were implemented in COMSOL Multiphysics. A non-isothermal flow was used. The generalized minimum residual method (GMRES) was used for the 3D model and the interpolation method for ambient

temperature was a cubic spline. For the air stream, the heat transfer coefficient was computed by the equation of Sieder and Tate, and then specified for the boundary conditions.

The Eq. (1) describes the heat transfer in the system studied:

$$\begin{cases} \rho \cdot C_p \dfrac{\partial T}{\partial t} + \rho \cdot C_p \cdot u \dfrac{\partial T}{\partial x} - K \dfrac{\partial^2 T}{\partial x^2} = 0 \\ \rho \cdot C_p \dfrac{\partial T}{\partial t} + \rho \cdot C_p \cdot u \dfrac{\partial T}{\partial y} - K \dfrac{\partial^2 T}{\partial y^2} = 0 \\ \rho \cdot C_p \dfrac{\partial T}{\partial t} + \rho \cdot C_p \cdot u \dfrac{\partial T}{\partial z} - K \dfrac{\partial^2 T}{\partial z^2} = 0 \end{cases} \quad (1)$$

Eq. (2) and Eq. (3) defined the momentum conservation for the fluid flow:

$$\frac{\partial u}{\partial x} + \frac{\partial v}{\partial y} + \frac{\partial w}{\partial z} = 0 \quad (2)$$

$$\begin{cases} u \dfrac{\partial u}{\partial x} + v \dfrac{\partial u}{\partial y} + w \dfrac{\partial u}{\partial z} = \vartheta \dfrac{\partial^2 u}{\partial x^2} - \dfrac{1}{p} \dfrac{\partial p}{\partial x} \\ u \dfrac{\partial v}{\partial x} + v \dfrac{\partial v}{\partial y} + w \dfrac{\partial v}{\partial z} = \vartheta \dfrac{\partial^2 v}{\partial y^2} - \dfrac{1}{p} \dfrac{\partial p}{\partial y} \\ u \dfrac{\partial w}{\partial x} + v \dfrac{\partial w}{\partial y} + w \dfrac{\partial w}{\partial z} = \vartheta \dfrac{\partial^2 w}{\partial z^2} + \rho \cdot g \end{cases} \quad (3)$$

The absorbed quantity of thermal energy from the PV/T can be calculated by Eq. (4):

$$Q_n = Q_{ab} + Q_{cv} + Q_{rd} \quad (4)$$

The heat loss on the top and bottom surfaces of the PV/T collector is given by Eq. (5):

$$Q_{cv} = h_w \cdot A_v \cdot \left(T_a - T_v\right) \quad (5)$$

Sumit and Tiwari [24] deduced that the convection transfer coefficient (h_w) depends on the airflow regime. It is written by Eq. (6):

$$h_w = 2{,}8 + 3 \times W_i \quad (6)$$

The amount of energy lost by radiation is calculated by Eq. (7), [25]:

$$Q_{rd} = \varepsilon_v \times \sigma \times A_v \times \left(T_a^{\,4} - T_v^{\,4}\right) \quad (7)$$

The thermal energy source is the amount of solar radiation absorbed by the PV/T. It is calculated by Eq. (8):

$$Q_{ab} = \alpha_v \times G \quad (8)$$

To solve the differential equations of heat transfer and airflow in the drying system studied, we apply the boundary conditions. The initial temperature at time $t = 0$, of the different components of the dryer is $T = T_0$. At the inlet of the collector, the air is unidirectional along the Z-axis with a variable temperature as a function of time. The two parameters are described by Eq. (9) and Eq. (10):

$$T_0 = T_{\text{int}}\left(t\right) \quad (9)$$

$$\begin{cases} u = 0 \\ v = 0 \\ w = V_e \end{cases} \quad (10)$$

A non-slip condition for the solid-fluid interfaces in the walls has been used, without viscous stress. It is described by Eq. (11):

$$\begin{cases} u = 0 \\ v = 0 \\ w = 0 \end{cases} \quad (11)$$

Thermal insulation of the studied system is written by Eq. (12):

$$-n\left(-K \nabla T\right) = 0 \quad (12)$$

For the upper surface of the glass cover, the condition is described by Eq. (13):

$$-K_v \times \Delta T_v\left(x, z\right) = hc_{v-a} \times \left(T_v - T_a\right) \quad (13)$$

The boundary condition at the back of the glass is defined by Eq (14):

$$\begin{cases} -K_v \dfrac{\partial T}{\partial z} = hc_{v-1} \times \left(T_v - T_1\right) \\ \text{and For} \\ x = 0, \dfrac{\partial T}{\partial x} = 0 \end{cases} \quad (14)$$

The boundary condition of the upper surface of the PV panel is described by Eq. (15):

$$\begin{cases} -K_{pv} \dfrac{\partial T}{\partial z} = hc_{pv-1} \times \left(T_{pv} - T_1\right) \\ \text{and For} \\ x = l, \dfrac{\partial T}{\partial x} = 0 \end{cases} \quad (15)$$

The boundary condition of the back surface of the PV panel is defined by Eq. (16):

$$\begin{cases} -K_{pv} \dfrac{\partial T}{\partial z} = hc_{pv-2} \times \left(T_{pv} - T_2\right) \\ \text{and For} \\ x = 0, \dfrac{\partial T}{\partial x} = 0 \end{cases} \quad (16)$$

At the back side of the PV/T air collector:

$$T = T_a \text{ and } x = l, \frac{\partial T}{\partial x} = 0 \quad (17)$$

The limit condition at the outlet of the dryer is defined by Eq. (18):

$$P = P_{atm} \quad (18)$$

4 RESULTS AND DISCUSSION

4.1 Metrologic Conditions

The climatic parameters measured are solar radiation ($G(t)$) and ambient temperature ($T_a(t)$) during the experiment in the city of Sfax, Tunisia.

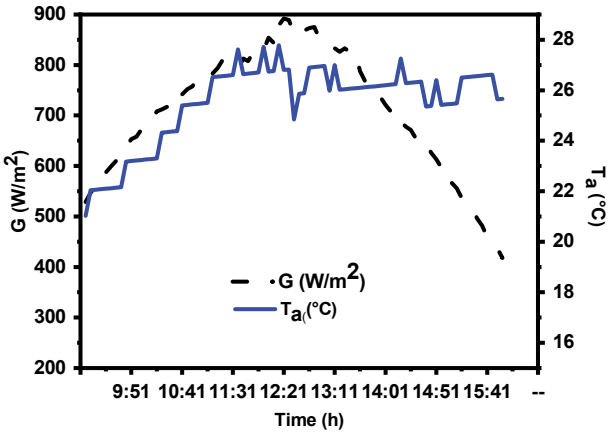

Figure 8 Experimental results of meteorological conditions

Fig. 8 shows the variation of these parameters during the day of the experiment. Solar radiation and ambient temperature present weather conditions that affect the thermal performance of the MSD. According to Fig.7, we notice that during the day, from sunrise to sunset, the solar radiation and the ambient temperature increase gradually and reach a maximum value at noon, then they decrease. The maximum values of the two parameters are recorded between 12:00 am and 2:00 pm, while during the experiment, the ambient temperature varies between (17 °C-30 °C) with solar radiation it varies from (300 W/m² to 900 W/m². Hence, the day is characterized by clear sky conditions.

4.2 3D Airflow Distribution in the Solar Dryer With PV/T

In order to have a clear understanding of the uniformity of air distribution in the drying system invented a study on the 3D distribution of air was carried. The results revealed are shown in Fig. 9 and Fig. 10.

These figures show that the airflow remains high only on the side of the drying chamber while between the trays, the airflow is weak. Hence, this condition will result in non-uniform removal of water from the product, where the product near the wall of the drying chamber will tend to evaporate the water faster than the one in the middle of the rack. Since the airflow delivered to the drying chamber has a maximum speed close to the inlet and the minimum speed in the center of the compartment, this indicates that the airflow is not homogeneous in the chamber. Perhaps, the drying chamber is oversized for this; a significant part of the air passes too far from the drying zone.

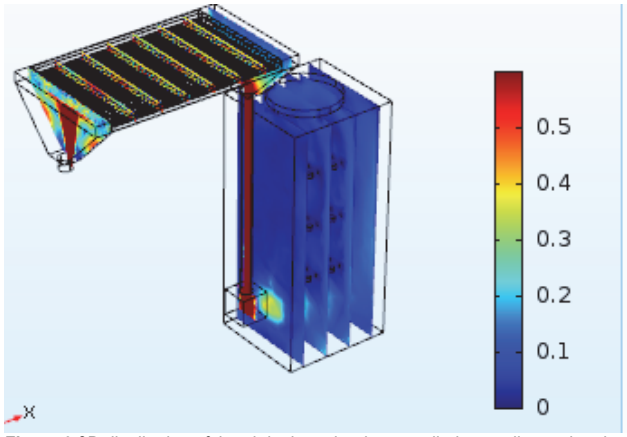

Figure 9 3D distribution of the air in the solar dryer studied according to the plan (*Y-Z*)

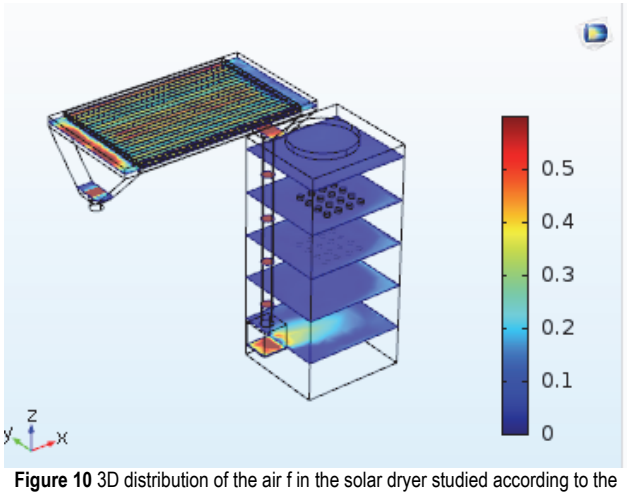

Figure 10 3D distribution of the air f in the solar dryer studied according to the plan (*X-Y*)

4.3 3D Distribution of Temperature in the Solar Dryer Studied

Fig. 11 illustrates the 3D distribution of the drying temperature inside the dryer. Firstly, the maximum temperature is recorded at noon, so the temperature in the drying chamber increases from sunrise to noon gradually. After that it decreases slowly to the sunset. Further, the temperature continues to increase inside the drying chamber in the afternoon due to the high thermal inertia of the PV/T. In addition, the recorded temperature is capable of drying certain food products such as tomatoes. Moreover, according to the numerical simulation, we can conclude that the distribution of the temperature in the chamber is almost homogeneous. Furthermore, the simulation shows that integrating the solar collector into the drying chamber is, therefore, a good idea because the drying temperature has improved thanks to the PV/T. Again, it can be seen in Fig. 11 that the temperature inside the dryer gradually increases respectively with the outlet temperature of the PV/T air collector during the day.

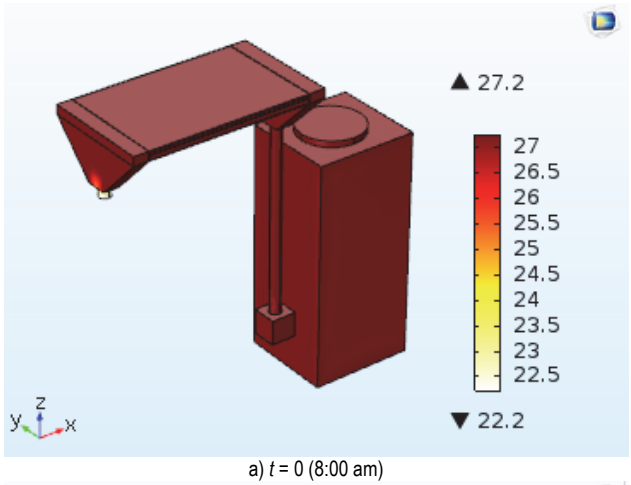

a) t = 0 (8:00 am)

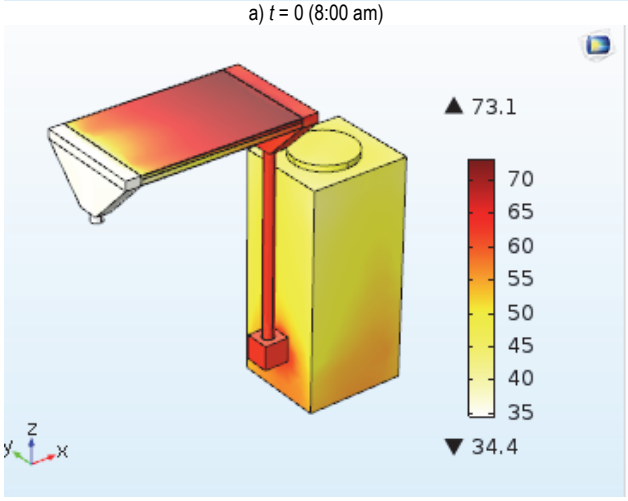

b) t = 4 h (12:00 am)

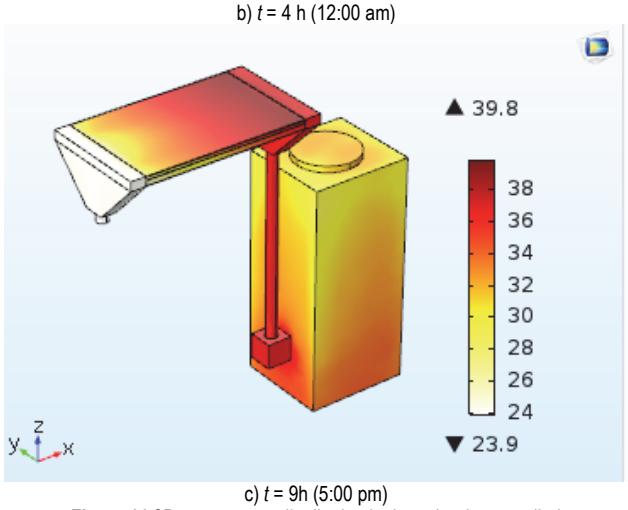

c) t = 9h (5:00 pm)

Figure 11 3D temperature distribution in the solar dryer studied

4.4 Experimental Airflow Distribution Inside the Drying Room

The distribution of air velocity in the drying chamber for all the trays is shown in Fig. 12. For each tray, the air speed was measured in five locations, two at the start of trays, one in the center of trays and two at the end of trays as shown in Fig. 4.

The experimental data shows a low speed in the trays placed in the lower half of the dryer compared to the trays situated in the upper half of the drying unit. However, low-speed regions in the lower trays caused a loss of energy and higher energy consumption. It can be concluded that the airflow is not homogeneous inside the chamber. The maximum air speed is always recorded in the middle of the tray.

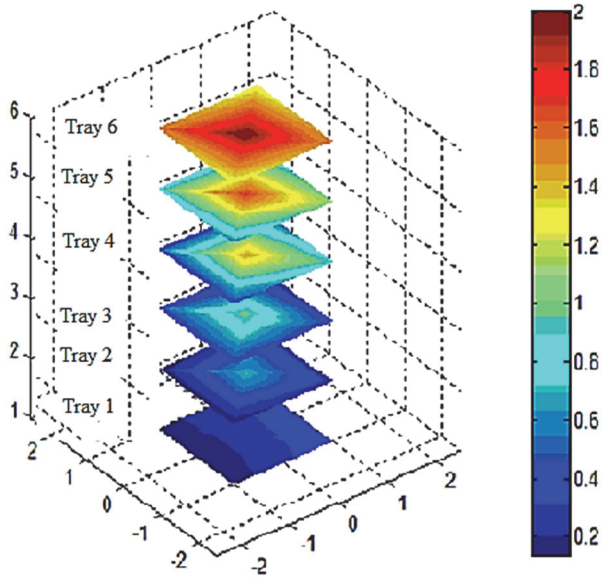

Figure 12 Experimental airflow distribution inside the drying chamber

4.5 Temperature Profiles of the Dryer

A comparison between the theoretical and experimental values of the temperatures in the glass, the air in the gap, PV panel, and outlet of the PV/T is given in Fig. 13. This figure shows an adequate agreement is predicted by the numerical results with the experimental data. A heating period exists during the first two hours from 9:00 am to 11:00 am, after which we identify the second period of thermal stabilization between 11:00 am and 2:00 pm Finally, the third period is well described as a cooling period.

It is clear from Fig. 13 that the temporal variation of temperatures has the same trends as solar radiation. This makes it possible to note that the temperatures of the PV/T varied proportionally as a function of the solar energy received by the solar collector PV/T. Consequently, the maximum temperature values were obtained between 12 noon and 2 p.m., then they gradually decrease. Further, we observe that the output temperature of the PV/T collector varies between 34 °C and 63 °C in the experience but it varied between 27 °C and 55 °C in the numerical simulation. Moreover, the PV cell temperature varies between 27,7 °C to 60 °C in the experimental, but it changed between 26,85 °C to 57,67 °C in the numerical solution. Furthermore, the temperature of the air gap fluctuates between 30,25 °C to 66,3 °C in the experience and it varied between 27 °C to 65,75 in the simulation. Likewise, the glass temperature varies between 32,56 °C to 68,8 °C and it changed between 26,85 °C to 67 °C in the experimental data and numerical simulation respectively. From the results, it is clearly seen that the air temperature of the PV/T at the outlet during the period 2:00 pm and 4:00 pm is relatively high, between 50 °C and 60 °C, even at 4:00 pm when the solar radiation is low. This is due to the thermal inertia of the PV/T. Hence, we note that the difference in ambient temperature and outlet temperature of the PV/T is strong. This is due to the strong absorption of solar radiation by the PV/T air collector.

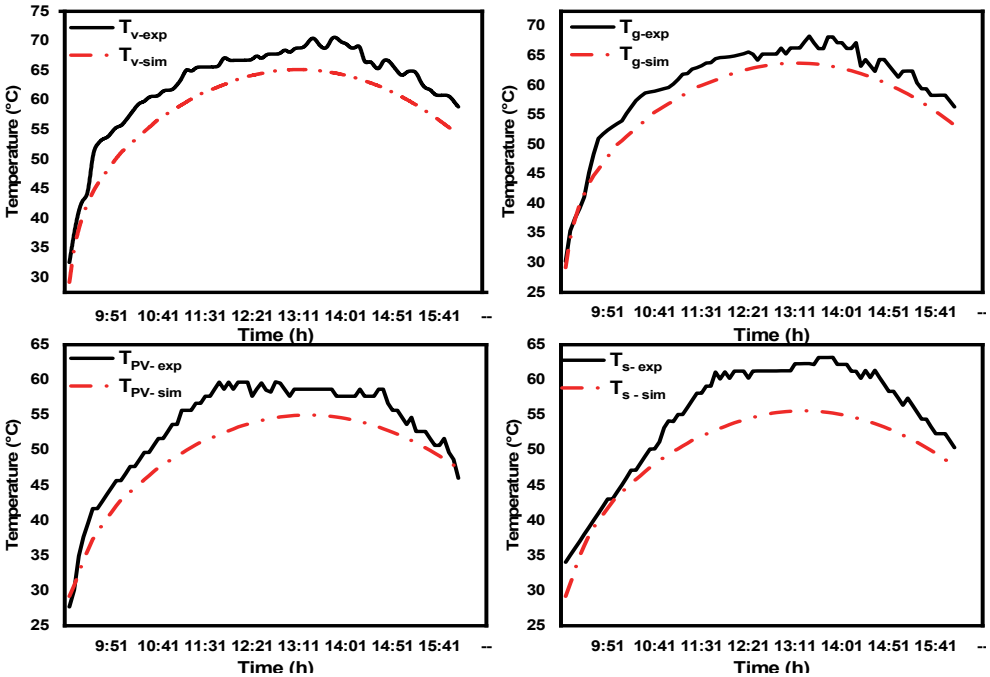

Figure 13 Experimental and numerical variation of the temperature of the PV/T for Q_m = 0,02 kg/s

The error analysis between the experimental values and the numerical simulation is grouped in Tab. 6. The results show that the maximum error is recorded at the start of the test due to the amount of heat stored in the PV/T before starting the experiment. Moreover, after an hour the amount of heat stored in the system has been absorbed by the air; however, the error is decreased to vary between 0,5% and 8%.

Table 6 Experimental and numerical values of temperatures in the PV/T for Q_m = 0,02 kg/s.

Temps (hours)	T_{v_exp}	T_{v_sim}	*Err* / %	T_{g_exp}	T_{g_sim}	*Err* / %	T_{Pv_exp}	T_{Pv_sim}	*Err* / %	T_{s_exp}	T_{s_sim}	*Err* / %
9:00 am	32,56	26,85	21,27	30,25	27,00	12,04	27,70	26,85	3,17	34,06	26,85	26,85
10:00 am	56,55	52,30	8,13	54,00	51,15	5,58	46,67	44,28	5,41	45,05	44,84	0,47
11:00 am	63,58	60,50	5,09	61,00	59,22	3,00	55,67	51,50	8,09	55,08	52,08	5,76
12:00 am	66,74	65,25	2,28	64,95	63,91	1,62	59,70	55,79	7,00	61,24	56,37	8,64
01:00 pm	68,80	67,03	2,64	66,30	65,72	0,88	58,65	57,67	1,70	61,30	58,21	5,31
02:00 pm	68,72	65,78	4,46	66,21	65,46	1,15	57,64	56,96	1,19	62,22	57,45	8,31
03:00 pm	64,89	61,58	5,37	62,39	60,53	3,07	53,65	53,78	0,25	56,39	54,19	4,06
04:00pm	58,85	54,39	8,20	56,35	53,58	5,17	46,00	48,18	4,52	50,35	48,47	3,88

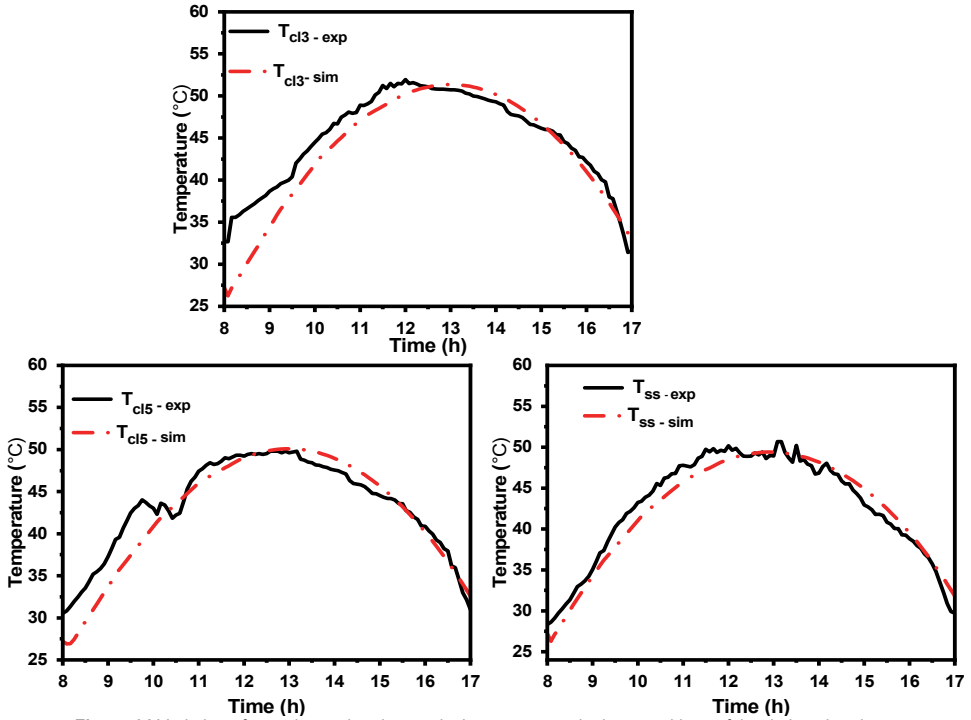

Figure 14 Variation of experimental and numerical temperatures in three positions of the drying chamber

Table 7 Experimental and numerical temperature values in three positions of the drying chamber

Temps (hours)	T_{cl3_exp}	T_{cl3_sim}	*Err* / %	T_{cl5_exp}	T_{cl5_sim}	*Err* / %	T_{ss_exp}	T_{ss_sim}	*Err* / %
9:00 am	38,68	34,41	12,42	37,27	33,71	10,55	35,06	34,20	2,51
10:00 am	44,49	41,83	6,35	40,02	40,84	5,33	43,26	41,03	5,43
11:00 am	48,90	47,17	3,68	47,42	46,02	3,04	47,78	45,84	4,24
12:00 am	51,96	50,25	3,39	49,22	49,03	0,38	50,17	48,55	3,35
01:00 pm	50,74	51,37	1,23	49,62	50,11	0,97	48,93	49,41	0,97
02:00 pm	49,31	50,18	1,72	47,56	48,97	2,87	46,84	48,18	2,77
03:00 pm	46,16	46,72	1,22	44,54	45,66	2,45	42,94	44,90	4,35
04:00 pm	42,17	41,01	2,82	40,89	40,22	1,67	38,82	39,52	1,78
05:00 pm	31,60	32,93	4,04	30,98	32,59	4,92	29,72	31,82	6,59

Fig. 14 shows the profiles of the experimental temperatures and the numerical simulation inside the drying chamber, such as the temperature of tray 3, the temperature of tray 5, and the outlet temperature of the dryer. The results have shown that the temperature grows progressively in the day until reaching a maximum value between 12:00 am and 2:00 pm; then it decreases slowly. Consequently, the temperature inside the drying chamber takes the same trend as the outlet temperature of the PV/T with a slight decrease that can be explained by the decrease in thermal inertia in the chamber due to the increase in the volume of the chamber. The temperature of tray 3 located in the middle of the chamber varied between a minimum of 38,68 °C and 51,96 °C for the experimental device and it changed from a minimum of 34,41 °C to a maximum of 51,37 °C for the simulation. Further, the temperature of the tray 5 varied between a minimum of 37,27 °C and 49,62 °C for the experimental device and it changed from a minimum of 33,71°C to a maximum of 50,11 °C for the simulation. In addition, the maximum outlet temperature of the drying chamber exceeds 50,17 °C and 49,41°C in the experiment and the numerical simulation respectively. We see that the simulation is in good agreement with the experimental results. This confirms that digital simulation is an adequate method to describe the behavior of a solar dryer. To enhance the numerical simulation, a credibility analysis is shown in Tab. 7. The results show that the maximum error of around 12,45% at the start of the experimental test can be explained by the amount of heat pumped from the PV/T. This amount of heat is due to the heat energy stored in the PV/T before starting the experiment. The numerical simulation has met with great success in comparison to experimental data. Likewise, the error varies between 0,38% and 12,47%.

4.6 Effect of the Mass Flow Rate on the Temperature Evolution of PV/T

Fig. 15 shows the influence of the mass flow rate (Q_m) for G = 650 W/m^2 and T_a = 30 °C on the variation of the outlet temperature and the PV panel temperature of the PV/T. The numerical simulation results show that the two temperatures decrease as the input velocity increases. In addition, when the input mass flow increases, the coefficient of heat exchange by convection between air and PV increases, consequently the heat is removed from the PV panel which causes the cooling of the photovoltaic cells and reduces their temperature. However, if the air flow rate increases from 0,012 kg/s to 0,025 kg/s, the outlet temperature drops from 60,5 °C to 44,7 °C and the temperature of the PV module varies from 63 °C for the lowest mass flow 0,012 kg/s to 43 °C for the highest mass flow 0,025 kg/s. However, in the numerical simulation, these two parameters changed from 62 °C to 45 °C and 63 °C to 47 °C respectively. So, it is advantageous to work with average flow rates in order to have slightly high temperatures at the output of the collector for drying and to ensure proper cooling of the PV module in order to improve their electrical performance.

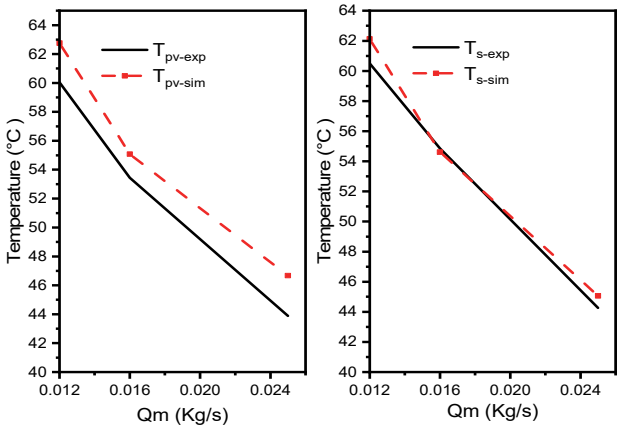

Figure 15 The temperatures profiles of the PV and the outlet of the PV/T under Q_m

Table 8 Experimental and numerical values of the outlet and PV cell temperatures of the PV/T

Q_m / kg/s	T_{s_exp}	T_{s_sim}	*Err* / %	T_{PV_exp}	T_{PV_sim}	*Err* / %
0,012	60,49	62,12	2,62	60,04	62,76	4,33
0,016	54,85	54,61	0,44	53,44	55,08	2,98
0,025	44,27	45,06	1,75	43,89	46,67	5,96

However, we observe a deviation from low airflow and a small deviation from high airflow. Nevertheless, a great agreement was observed between the experimental and numerical results. The error values are shown in Tab. 8, they vary between 0,44% and 5,96%.

4.7 Effect of the Solar Radiation on the Temperature Evolution of PV/T

One of the major topics investigated in this paper is the effect of solar radiation on the evolution of the outlet temperature (T_s) and photovoltaic panel temperature (T_{pv}). The impact of solar radiation on the evolution of the T_{pv} and T_s of the PV/T shown in Fig. 16 for Q_m = 0,0166 kg/s and T_a = 25 °C. It is clear from the results revealed by the experimental data and numerical simulation that the increase in solar radiation generates an increase in temperatures T_s and T_{pv}. Hence, we notice that there is a difference in amplitude between the air temperature of the outlet (T_s), and the PV temperature (T_{pv}). This difference is expected since part of the solar energy received by the PV panel is kept there in electricity and is not transmitted to

heat. Moreover, the results show that the two temperatures vary linearly with the solar radiation. In addition, what can be explained is the fact that the part of the flux of solar radiation received by the solar air collector to heat the quantity of air depends on the daylight.

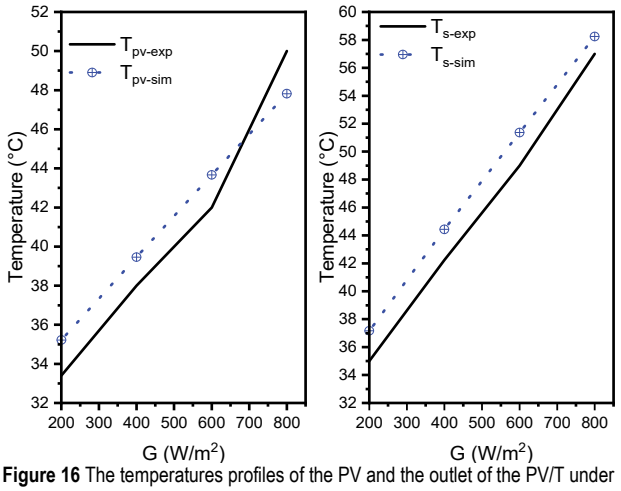

Figure 16 The temperatures profiles of the PV and the outlet of the PV/T under *G*

The temperatures (T_s) and (T_{pv}) of the PV/T vary between 35 °C and 57 °C, 33,5 °C and 50 °C respectively for solar radiation, which varies between 200 and 800 W/m^2. However, increasing the PV module temperature has a negative effect on the electrical performance of the system studied. The growth of the PV/T outlet temperature due to the sunshine has a positive impact on the thermal efficiency of the PV/T. This implies that an increase in solar radiation leads to an improvement in thermal efficiency but decreases the electrical performance of the module.

4.8 Effect of the Mass Flow Rate on the Thermal Efficiency

The thermal efficiency of the PV/T calculated by the Eq. (20) was solved numerically and examined experimentally according to the effect of mass flow rate. Note that the efficiency is a little high at the start of the experimental test due to the energy stored in the PV/T before the start of the experimental equipment when the airflow is stagnant. Furthermore, it is clear that the thermal performance gradually increases with sunlight.

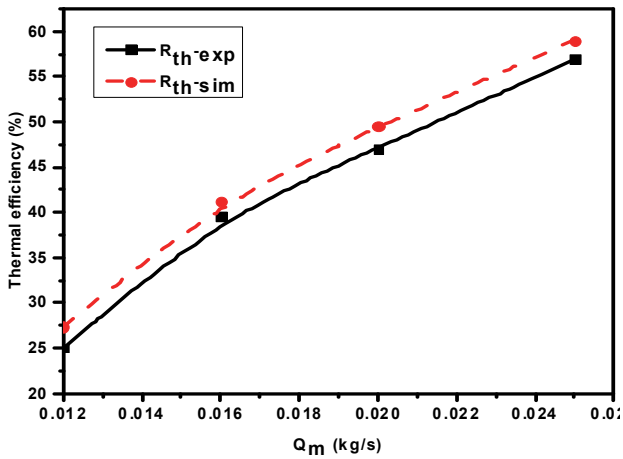

Figure 17 Average thermal efficiency of the PV/T

$$R_{th} = \frac{Q_{th}}{A_c \times \int G \, dt} \tag{19}$$

$$Q_{th} = Q_m \times C_p \times \Delta T \tag{20}$$

Table 9 Experimental and numerical average values of thermal efficiency

Q_m / kg/s	R_{th_exp}	R_{th_sim}	Err / %
0,012	25,02	27,40	8,68
0,016	39,55	41,24	4,10
0,02	47,06	49,50	4,94
0,025	56,90	59,00	3,56

The results from experimental data and numerical simulation are shown in Fig. 17 and they reveal that the best experimental thermal efficiency recorded is 56,9% for the maximum mass flow rate of 0,025 kg/s. Hence, it reaches 59% for the numerical simulation. Likewise, the experimental and numerical thermal yields are respectively 25,02% and 27,4%, if the airflow decreases to 0,012 kg/s. So, it can be concluded that the performance of air PV/T is significantly affected by the air mass flow rates. Also, it can be clearly seen that the treatment of the PV/T collector with a tube structure has shown an improvement in the thermal performance. The values of experimental results and numerical simulations and the error calculation are shown in Tab. 8. However, the error percentage between numerical and experimental values in terms of thermal efficiency varies between 8,68% for Q_m = 0,012 kg/s and 3,56% for Q_m = 0,025 kg/s.

5 CONCLUSIONS

A solar dryer with a PV/T air collector was studied experimentally and its mathematical model was solved numerically. From the study, we conclude that the simulation is able to follow and predict the temperature evolution, and examine the airflow distribution inside the solar dryer. In addition, we can follow the effect of the various possible operating conditions without having to perform the physical experiment, which is sometimes time-consuming and expensive.

As a result, we can see that the performance remains increasing despite the decrease in the sunshine in the afternoon, which explains the fact that the quantity of heat pumped from the solar collector is greater than that absorbed, which ensures a longer drying time during the day. Further, the improvement of the mass flow rate dropped approximately the average PV temperature experimentally from 60 °C to 43 °C, then from 63 °C to 47 °C numerically. Moreover, the average outlet temperature of the PV/T reaches 60,5 °C in the experience and 62 °C in the simulation in the case where the mass flow rate is 0,012 kg/s, but it dropped to 44 °C in the experience and 45 °C in the simulation for the highest mass flow rate 0,0235 kg/s. Hence, the best recorded average thermal efficiency of the PV/T was 53% for the maximum mass flow rate (0,025 kg/s), while the average thermal efficiency of the PV/T was 29% when the mass flow rate decreased to 0,012 kg/s. Consequently, the recorded temperature in the drying chamber reaches 55 °C in the experimental data and in the numerical simulation. Thus, the incorporation of the PV/T solar collector with a solar dryer is a good idea. As a result, the solar dryer with PV/T is able to dry some vegetables and fruits such as tomatoes.

Acknowledgements

The authors extend their appreciation to the Deputyship for Research & Innovation, Ministry ofEducation in Saudi Arabia for funding this research work through the project number "IF_2020_NBU_409". The authors gratefully thank the Prince Faisal bin Khalid bin Sultan Research Chair in Renewable Energy Studies and Applications (PFCRE) at Northern Border University for their support and assistance.

6 REFERENCES

[1] El Hage, H., Herez, A., Ramadan, M., Bazzi, H., & Khaled, M. (2018). An investigation on solar drying: A review with economic and environmental assessment. *Energy*, *157*, 815-829. https://doi.org/10.1016/j.energy.2018.05.197

[2] Chauhan, P. S., Kumar, A., & Tekasakul, P. (2015). Applications of software in solar drying systems - a review. *Renewable and Sustainable Energy Reviews*, *51*, 1326-1337. https://doi.org/10.1016/j.rser.2015.07.025

[3] Kudra, T. & Mujumdar, A. S. (2009). *Advanced drying technologies*. CRC press.

[4] Kumar, M., Sansaniwal, S. K., & Khatak, P. (2016). Progress in solar dryers for drying various commodities. *Renewable and Sustainable Energy Reviews*, *55*, 346-360. https://doi.org/10.1016/j.rser.2015.10.158

[5] Punlek, C., Pairintra, R., Chindaraksa, S., & Maneewan, S. (2009). Simulation design and evaluation of hybrid PV/T assisted desiccant integrated HA-IR drying system (HPIRD). *Food and Bioproducts Processing*, *87*(2), 77-86. https://doi.org/10.1016/j.fbp.2008.10.002

[6] Jia, Y., Alva, G., & Fang, G. (2019). Development and applications of photovoltaic-thermal systems - a review. *Renewable and Sustainable Energy Reviews*, *102*, 249-265. https://doi.org/10.1016/j.rser.2018.12.030

[7] Fterich, M., Chouikhi, H., Bentaher, H., & Maalej, A. (2018). Experimental parametric study of a mixed-mode forced convection solar dryer equipped with a PV/T air collector. *Solar Energy*, *171*, 751-760. https://doi.org/10.1016/j.solener.2018.06.051

[8] César, L.-V. E., Lilia, C.-M. A., Octavio, G.-V., Isaac, P. F., & Rogelio, B. O. (2020). Thermal performance of a passive, mixed-type solar dryer for tomato slices (Solanum lycopersicum). *Renewable Energy*, *147*, 845-855. https://doi.org/10.1016/j.renene.2019.09.018

[9] Elkhadraoui, A., Kooli, S., Hamdi, I., & Farhat, A. (2015). Experimental investigation and economic evaluation of a new mixed-mode solar greenhouse dryer for drying of red pepper and grape. *Renewable energy*, *77*, 1-8. https://doi.org/10.1016/j.renene.2014.11.090

[10] Sreekumar, A., Manikantan, P., & Vijayakumar, K. (2008). Performance of indirect solar cabinet dryer. *Energy Conversion and Management*, *49*(6), 1388-1395. https://doi.org/10.1016/j.enconman.2008.01.005

[11] Kam, S., Kombasseré, A. M., Kaboré, B., Ouedraogo, G. W. P., & Bathiébo, D. J. (2017). Numerical simulation of greenhouse solar dryer in natural convection. *International Journal of Development Research*, *7*(12), 18005-18009.

[12] Kuan, M., Shakir, Y., Mohanraj, M., Belyayev, Y., Jayaraj, S., & Kaltayev, A. (2019). Numerical simulation of a heat pump assisted solar dryer for continental climates. *Renewable Energy*, *143*, 214-225. https://doi.org/10.1016/j.renene.2019.04.119

[13] Daghigh, R., Shahidian, R., & Oramipoor, H. (2020). A multistate investigation of a solar dryer coupled with photovoltaic thermal collector and evacuated tube collector. *Solar Energy*, *199*, 694-703. https://doi.org/10.1016/j.solener.2020.02.069

[14] Lakshmi, D., Muthukumar, P., Layek, A., & Nayak, P. K. (2019). Performance analyses of mixed mode forced convection solar dryer for drying of stevia leaves. Solar *Energy*, *188*, 507-518. https://doi.org/10.1016/j.solener.2019.06.009

[15] Simo-Tagne, M., Zoulalian, A., Rémond, R., & Rogaume, Y. (2018). Mathematical modelling and numerical simulation of a simple solar dryer for tropical wood using a collector. *Applied Thermal Engineering*, *131*, 356-369. https://doi.org/10.1016/j.applthermaleng.2017.12.014

[16] Bennamoun, L. & Belhamri, A. (2006). Numerical simulation of drying under variable external conditions: application to solar drying of seedless grapes. *Journal of Food Engineering*, *76*(2), 179-187. https://doi.org/10.1016/j.jfoodeng.2005.05.005

[17] Dhalsamant, K., Tripathy, P., & Shrivastava, S. (2018). Heat transfer analysis during mixed-mode solar drying of potato cylinders incorporating shrinkage.Numerical simulation and experimental validation. *Food and Bioproducts Processing*, *109*, 107-121. https://doi.org/10.1016/j.fbp.2018.03.005

[18] Kasaeian, A., Khanjari, Y., Golzari, S., Mahian, O., & Wongwises, S. (2017). Effects of forced convection on the performance of a photovoltaic thermal system - an experimental study. *Experimental Thermal and Fluid Science*, *85*, 13-21. https://doi.org/10.1016/j.expthermflusci.2017.02.012

[19] Aissaoui, F., Benmachiche, A. H., Brima, A., Bahloul, D., & Belloufi ,Y. (2016). Experimental and theoretical analysis on thermal performance of the flat plate solar air collector. *International Journal of Heat and Technology*, 34(2), 213-220. https://doi.org/10.18280/ijht.340209

[20] Koşan, M., Demirtaş, M., Aktaş, M., & Dişli, E. (2020). Performance analyses of sustainable PV/T assisted heat pump drying system. *Solar Energy*, *199*, 657-672. https://doi.org/10.1016/j.solener.2020.02.040

[21] Armstrong, S. & Hurley, W. (2010). A thermal model for photovoltaic panels under varying atmospheric conditions. *Applied Thermal Engineering*, *30*(11-12), 1488-1495. https://doi.org/10.1016/j.applthermaleng.2010.03.012

[22] Notton, G., Cristofari, C., Mattei, M., & Poggi, P. (2005). Modelling of a double-glass photovoltaic module using finite differences. *Applied thermal engineering*, *25*(17-18), 2854-2877. https://doi.org/10.1016/j.applthermaleng.2005.02.008

[23] Jones, A. & Underwood, C. (2001). A thermal model for photovoltaic systems. *Solar energy*, *70*(4), 349-359. https://doi.org/10.1016/S0038-092X(00)00149-3

[24] Tiwari, S. & Tiwari, G. (2017). Energy and exergy analysis of a mixed-mode greenhouse-type solar dryer, integrated with partially covered N-PVT air collector. *Energy*, *128*, 183-195. https://doi.org/10.1016/j.energy.2017.04.022

[25] Aktaş, M., Şevik, S., Amini, A., & Khanlari, A. (2016). Analysis of drying of melon in a solar-heat recovery assisted infrared dryer. *Solar Energy*, *137*, 500-515. https://doi.org/10.1016/j.solener.2016.08.036

LIST OF ABBREVIATIONS

MSD	Mixed solar dryer
OSD	Open solar dryer
PV/T	Photovoltaic-thermal collector
PV	Photo Voltaic panel
G	Solar radiation / W/m²
Q_m	Masse flow rate / kg/s
T	Time (s)
k	thermal conductivity / W/Km
Q_n	Heat net / W
Q_c	Convective heat loss / W
Q_{ab}	Heat source absorber / W

Q_{rd}	Radiation heat loss / W
Q	Total heat generation / W
Re	Reynolds number
Nu	Nusselt number
Pr	prandt number
R_{th}	Thermal efficiency / %
T	Temperature / °C
$hc_{v\text{-}1}$	Convection heat transfer coefficient between glass and air gap / W/m²K
$hc_{pv\text{-}1}$	Convection heat transfer coefficient between PV and air gap / W/m²K
$hc_{pv\text{-}2}$	Convection heat transfer coefficient between PV and air tube coefficient / W/m² K
h_r	Radiative heat transfer coefficient / W/m² K
h_w	Convection heat transfer coefficient between glass and ambient / W/m² K
σ	Stefan-Boltzmann constant / W/m²K^4)
U	Velocity field / m/s
∇	Vector differential operator
u	Air flow velocity in the x direction / m/s
v	Air flow velocity in the y direction / m/s
w	Air flow velocity in the z direction / m/s
A	Area / m²
D_h	Hydraulic diameter / m
x, y	Space coordinates
W_i	Wind velocity / m/s
ϑ	Kinematic viscosity / m²/s
∇	Vector differential operator
Cp	Specific heat capacity / J/kg°C
K	Thermal conductivity / W/mK
V_e	Inlet velocity / m/s
μ	Dynamic viscosity of the fluid / kg/ms
L_{eq}	Length equivalent / m
I	Moment of inertia / kgm²
F	Volume force / N
g	Gravity field / m/s^2
S	Section / m²
P	Static pressure / Pa
ΔP	Pressure drop / Pa

Greek Symbols

Err	Error (%)
α	Absorptivity
ε	Emissivity
τ	Transmissivity
σ	Stefan-Boltzmann constant / W/m²K^4
ρ	Density / kg/m^3

Subscripts

exp	Experimental
sim	Simulation
s	Outlet
cl3	Tray number 3
cl5	Tray number 5
ss	Outlet dryer
a	Ambient
v	Glass
g	Gap
1	Air between glass and PV
2	Air inside the tube
int	Inlet

Contact Information:

Mohamed FTERICH, Lecturer
(Corresponding author)
Department of Industrial Engineering, College of Engineering,
Northern Border University,
Arar, Saudi Arabia
E-mail: mohamed.fterich@enis.tn

Houssam CHOUIKHI, Assistant Professor
University of Sfax, National School of Engineers of Sfax,
Laboratory of Electromechanical Systems (LASEM), URL, 3038 Sfax, Tunisia
Mechanical Engineering Department, College of Engineering,
King Faisal University, Kingdom of Saudi Arabia
E-mail: h.chouikhi@gmail.com

Salmen GHORBEL, PhD Student
University of Sfax, National School of Engineers of Sfax,
Laboratory of Electromechanical Systems (LASEM), URL, 3038 Sfax, Tunisia
E-mail: Salmen.ghorbel1@gmail.com

Hatem BENTAHER, Associate Professor
University of Sfax, National School of Engineers of Sfax,
Laboratory of Electromechanical Systems (LASEM), URL, 3038 Sfax, Tunisia
E-mail: bentaherh@yahoo.com

Sadoth SANDOVAL TORRES, Professor
Instituto Politécnico Nacional - CIIDIR Oaxaca. Hornos 1003,
Santa Cruz Xoxocotlán, Oaxaca, Oax, CP 71230, Mexico
E-mail: sadoth.sandoval@gmail.com

Aref MAALEJ, Professor
University of Sfax, National School of Engineers of Sfax,
Laboratory of Electromechanical Systems (LASEM), URL, 3038 Sfax, Tunisia
Department of Electrical and Electronic Engineering Science,
University of Johannesburg, Johannesburg 2006, South Africa
E-mail: aref.maalej1@gmail.com